TOPOLOGICAL OPTICS

Topological insulator vertical-cavity laser array

Alex Dikopoltsev[1]†, Tristan H. Harder[2]†, Eran Lustig[1], Oleg A. Egorov[3], Johannes Beierlein[2], Adriana Wolf[2], Yaakov Lumer[1], Monika Emmerling[2], Christian Schneider[4], Sven Höfling[2], Mordechai Segev[1]*, Sebastian Klembt[2]*

Topological insulator lasers are arrays of semiconductor lasers that exploit fundamental features of topology to force all emitters to act as a single coherent laser. In this study, we demonstrate a topological insulator vertical-cavity surface-emitting laser (VCSEL) array. Each VCSEL emits vertically, but the in-plane coupling between emitters in the topological-crystalline platform facilitates coherent emission of the whole array. Our topological VCSEL array emits at a single frequency and displays interference, highlighting that the emitters are mutually coherent. Our experiments exemplify the power of topological transport of light: The light spends most of its time oscillating vertically, but the small in-plane coupling is sufficient to force the array of individual emitters to act as a single laser.

Topological insulators are systems that exhibit edge conductance that is protected against disorder and defects. Initially, this concept was related to electrons in solids, but this plentiful phenomenon was recently demonstrated in many wave systems such as photonics, cold atoms, and acoustics. Several years after establishing that topological properties can endow the transport of light with immunity against scattering from imperfections, the use of topological platforms to force injection locking of many semiconductor laser emitters was suggested. It was proposed (*1*, *2*) that the proper design of a multilaser array can lead to an edge mode flowing from one laser to another; force injection locking, despite some inevitable variations in the resonators; and eventually make all the elements lase as a single coherent source. This idea was demonstrated (*3*, *4*) in an array of asymmetrically coupled ring resonators (*5*), with standard semiconductor laser technology. Sequentially, topological lasing using magneto-optic materials was demonstrated (*6*). Since then, topological insulator lasers were demonstrated in a variety of configurations (*7*–*11*), for example, a topological quantum cascade laser with valley edge modes (*7*), a topological bulk laser based on band inversion–induced reflection (*8*), a spin-momentum-locked topological laser (*9*), and a topological insulator laser with next-nearest-neighbor coupling (*10*). Moreover, recent theoretical work has shown the dramatically reinforced coherence of topological lasers compared with the corresponding nontopological devices (*12*). The topological insulator laser is thus a promising application of topological photonics, and many new ideas have emerged, for example, using topology in synthetic dimensions to force an array of semiconductor lasers to emit mode-locked pulses (*13*).

The main reasons why topological properties make this possible are as follows. First, the topological edge mode in all topological insulator systems has a nonzero group velocity; hence, it must flow between lasers. As such it forces injection locking of all emitters associated with the edge mode while suppressing independent lasing of localized groups of resonators. Second, the topological platform guarantees robustness against small differences between resonators that would reduce the efficiency of injection locking.

Forcing injection locking of a large array of lasers has been a challenge for decades. The first attempts to combine several semiconductor lasers used evanescently coupled one-dimensional (1D) arrays of edge emitters (*14*, *15*). However, these arrays emitted light with unstable modal structure, and their mutual coherence diminished when the number of emitters was larger than just a few lasers (*16*–*19*). A decade later, 2D arrays of evanescently coupled vertical-cavity surface-emitting lasers (VCSELs) were investigated (*20*, *21*). However, despite tour-de-force attempts to make coherent arrays of many VCSELs (*22*–*24*), large VCSEL arrays are now being used only in a mutually incoherent form. This means that such VCSEL arrays can be used, for example, to pump solid-state lasers but not for any application requiring coherence, interference, imaging, and the like. Obviously, finding a way to make large arrays of VCSELs act together as a single coherent source would enable applications that are beyond current technology.

Our topological insulator VCSEL array is designed to form a closed topological interface containing 30 emitters (Fig. 1). The structure is fabricated by molecular beam epitaxial growth of a quantum-dot gain medium (*25*) embedded in a single wavelength cavity layer sandwiched between two distributed Bragg reflectors (DBRs). The lattices are defined using electron-beam lithography and subsequent dry etching. Each VCSEL is a circular micropillar, a shape that, in principle, can support more than one polarization-dependent mode. However, as the diameter decreases in size, the spectral spacing between the modes increases, and the VCSEL tends to lase in a single polarization (*26*, *27*). We use the small diameter d = 2.5 μm and lattice constant $3a$ = 6.5 μm [for details, see (*28*)]. The VCSELs are ordered in the topological geometry known as the "crystalline" model (*29*–*33*) (Fig. 2A), where the topological nature arises from different geometries on both sides of an interface between "stretched" and "compressed" honeycomb lattices. Both lattices are achieved by stretching or compressing the distances inside a unit cell of six sites. In the compressed

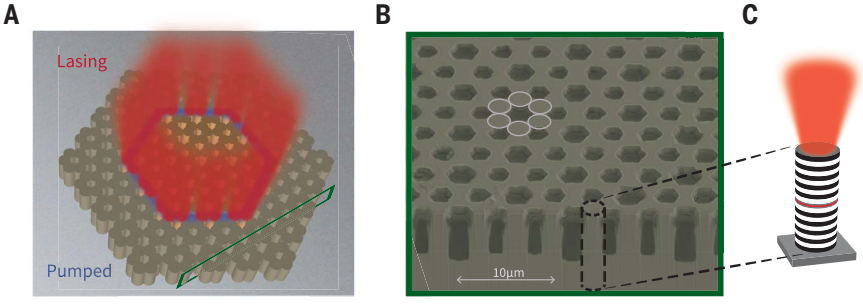

Fig. 1. Topological insulator VCSEL array. (**A**) Topological insulator VCSEL array, composed of two types of lattices: compressed and stretched honeycomb lattices, on either side of the topological interface. When the array is pumped on the interface (blue), the 30 VCSELs on the topological edge are injection-locked and lase vertically and coherently. (**B**) Scanning electron microscope image of the fabricated structure. Each pillar is a vertical microcavity, and the planar arrangement is based on the crystalline model with a six-pillar unit cell (white circles). (**C**) A single VCSEL: gain medium (red layer) sandwiched between two DBRs. Light emission is vertical.

[1]Physics Department, Technion, 32000 Haifa, Israel. [2]Technische Physik, Wilhelm-Conrad-Röntgen-Research Center for Complex Material Systems, and Würzburg-Dresden Cluster of Excellence ct.qmat, Universität Würzburg, Am Hubland, D-97074 Würzburg, Germany. [3]ITFO, Abbe Center of Photonics, Friedrich-Schiller-Universität Jena, D-07743 Jena, Germany. [4]Institute of Physics, University of Oldenburg, D-26129 Oldenburg, Germany.
***Corresponding author. Email: msegev@technion.ac.il (M.S.); sebastian.klembt@uni-wuerzburg.de (S.K.)**
†These authors contributed equally to this work.

lattice, the six pillars in each unit cell are separated by radius r_1 from the center, where $r_1 < a$ (a is the distance in the honeycomb before the compression); in the stretched lattice, the distances are $r_2 > a$. The stretching and compression open bandgaps at the Dirac points of the underlying honeycomb lattice, and each lattice has a different topological invariant. The interface therefore supports topological edge states [see explanation and fig. S1 in (*28*)]. Figure 2B presents such a topological state that resides on the interface. To view the band structure of the two lattice bulks and of the topological interface, we obtain their Fourier space luminescence spectra along the K-Γ-K′ direction of the underlying honeycomb lattice (Fig. 2, C to E). When the bandgap of the "stretched" bulk array is aligned with the bandgap of the "compressed" bulk array, the interface exhibits a 553-μeV-wide topological gap. As Fig. 2D shows, new modes appear at the interface—the topological edge modes, which are known to display topological protection properties (*30*). These topological edge modes have group velocities whose direction depends on their intra–unit cell pseudo-spin, which in closed interface paths may carry orbital angular momentum (*33*). As shown in (*28*), we calculate the band structure of the system by using a continuous model for the envelope of the light field in the micropillar photonic cavities. This model entails rich physics; for example, it describes well all the photonic states of the array, including photonic bands composed of higher modes within each pillar. Comparing experiments with simulations, we find good agreement, highlighting that the modes in the gap are edge modes with nonzero group velocity.

Our VCSEL array lases in a topological edge mode of 30 VCSELs located on the topological interface (Fig. 3A). To drive lasing of the edge mode, we pump the interface with a pulsed hexagon-shaped beam using a spatial light modulator and measure the lasing pattern and spectrum [for more details, see (*28*)]. By imaging the out-of-plane optical output, we find that lasing occurs precisely at the topological interface composed of the 30 VCSELs on the edge (Fig. 3B). The lasing intensity structure is not uniform because of inevitable fabrication imperfections and the nonuniform position of the quantum dots in the gain layer within each pillar. However, despite the nonuniform lasing, the topological platform forces all the emitters on the topological interface to lock and lase as a single laser (rather than lasing in several independent localized groups), as we show next. Figure 3C presents the emission spectrum below and above the lasing threshold. When we pump below the lasing threshold, the broad emission spectrum implies that multiple modes emit amplified spontaneous emission. When the pumping is above the lasing threshold, we observe single-mode lasing exactly at the wavelength of the topologically protected modes. The lasing topological mode maintains a narrow emission spectrum at a stable energy with a 249-μeV linewidth, which is less than half the width of the topological bandgap in our system (553 μeV). Moreover, the lasing linewidth of a single individual VCSEL in our array is ~170 μeV. This means that our 30-emitter VCSEL array lases with a linewidth almost as narrow as that of a single emitter in the array. Figure 3D shows the light output as a function of the input pump power, with a pumping threshold of $P_{th} \sim 25$ mW.

An important ingredient of coherence, especially when dealing with multi-emitters, is the interference between emitters located far apart from each other. To show the coherence of the lasing topological edge mode, we measure the interference of the output field with its mirror image around $x = 0$ (Fig. 3E) [setup described in (*28*)]. By doing this, we interfere the fields of every two VCSELs located on either side of the mirror axis. In this setting, the periodicity of the interference fringes arises mostly from the angle between the two arms of the interferometer. Specifically, the measured fringes in regions III and IX in Fig. 3E are the outcome of interference between VCSELs from region 3 and VCSELs from region 9 from Fig. 3A. The fringes in region VI in Fig. 3E are the result of the interference between VCSELs in region 6 and themselves. Importantly, the interference in regions III and IX is between VCSELs located 13 emitters and three corners apart from one another. This figure shows that every emitter interferes with its counterpart, showing that the coherence across the array is able to reestablish within each pumping cycle (even better results are expected with electrical pumping). The interference fringes are evidence that all 30 VCSELs act as a single coherent emitter.

Next, we compare the topological insulator VCSEL array with a trivial honeycomb VCSEL array (taking r_1, $r_2 \rightarrow a$) (Fig. 4) while exciting the trivial lattice with the same pump beam. Figure 4A shows the calculated band structure for the s- and p-bands, corresponding to the first and second modes of a single pillar, respectively. In both lattices, the measured spectrum corresponds to the modes with the maximum calculated overlap with the shaped pump beam. The measured spectrum of the topological array is localized in the topological gap, where the group velocity of the topological edge modes is high. By contrast, the spectrum of the trivial array is mainly located at the bottom of the p-band bulk, especially at the band edges where the group velocity goes to zero. The zero group velocity of the lasing modes in the trivial array means that localized groups of VCSELs tend to lase independently, in contrast to the topological array where the edge modes cannot be stationary. The wave in the topological mode has to circulate around the edge,

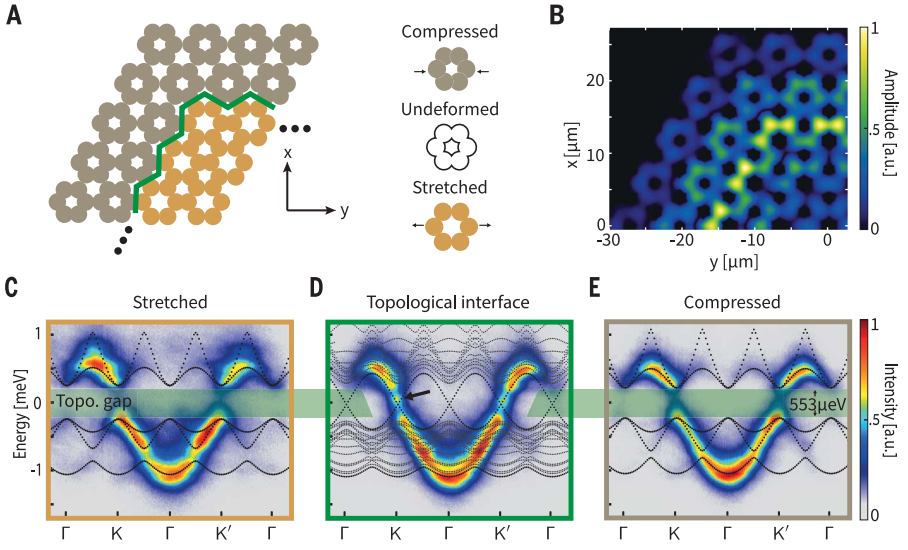

Fig. 2. Structure and photonic properties of the topological interface. (**A**) VCSEL array structure, composed of compressed (gray) and stretched (yellow) six-pillar unit cells of deformed honeycomb lattices, with uniform pillar-shaped VCSELs. The green line marks the topological interface. (**B**) Topologically protected mode centered on the interface between the two lattice types. a.u., arbitrary units. (**C** to **E**) Fourier-space photoluminescence spectra for the stretched bulk (C), topological interface (D), and the compressed bulk (E). The measured spectra are overlaid on the calculated band structure (black lines). The vertical axis is normalized so that 0 corresponds to 1.3003 eV, exactly the center of the topological gap. Note the measured photoluminescence peak from the photonic states in the topological gap [black arrow in (D)], exactly where the two bulk spectra [(C) and (E)] have bandgaps.

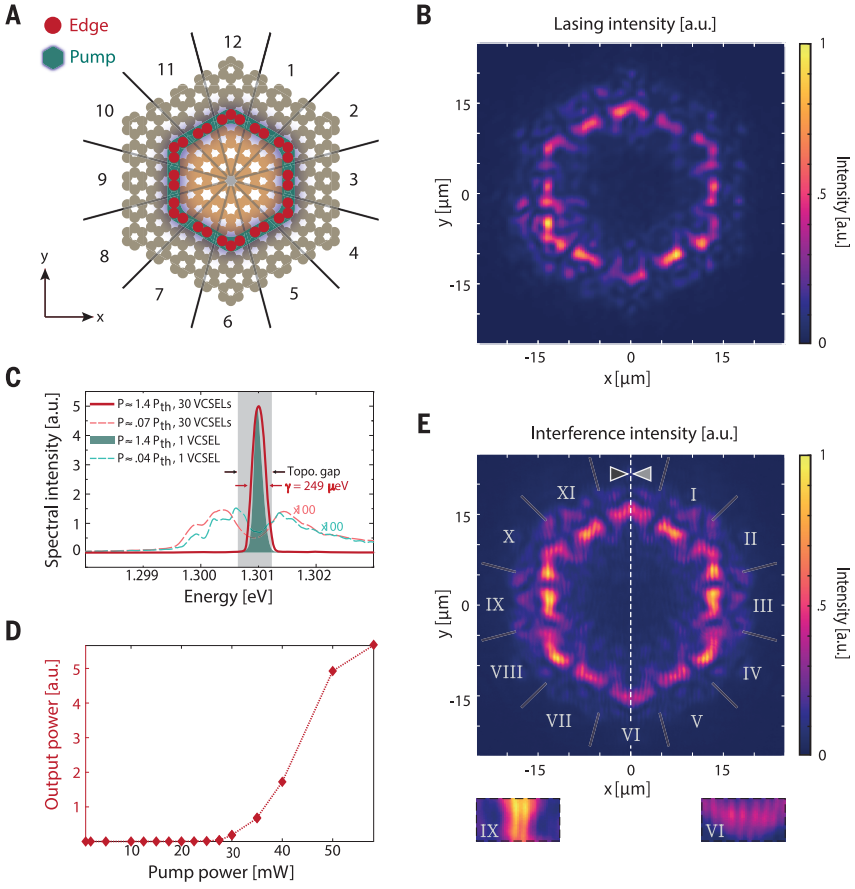

Fig. 3. Collective coherent lasing of the 30 VCSELs on the interface in the topological insulator array. (**A**) The topological VCSEL array. The inner bulk (yellow) (outer bulk, gray) is obtained by stretching (compressing) the honeycomb lattice. We pump the VCSELs on the topological interface (red) between the two bulks. (**B**) Lasing intensity of the topological edge mode. The shape includes corners and inevitable inhomogeneity, but the lasing is relatively uniform all along the topological edge. (**C**) Lasing spectrum of the topological array. The output spectra of a single VCSEL and the 30 VCSELs of the array are practically the same, below and above the lasing threshold. The measured lasing spectrum of the topological array (red line) is narrow (249 μeV) and fully contained within the topological gap (shaded region). (**D**) Output power versus pump power. (**E**) Interference between the lasing field and its mirror image, which measures coherence between lasers symmetrically located around $x = 0$. The fringes in region VI arise from interfering lasers in region 6 [of (A)] with themselves. The fringes in region IX show interference between the distinct lasers from regions 3 and 9 [of (A)]. Regions III and IX show interference fringes, even though emitters 3 and 9 are 13 VCSELs apart. The insets show zoom-ins of the fringes in regions VI and IX.

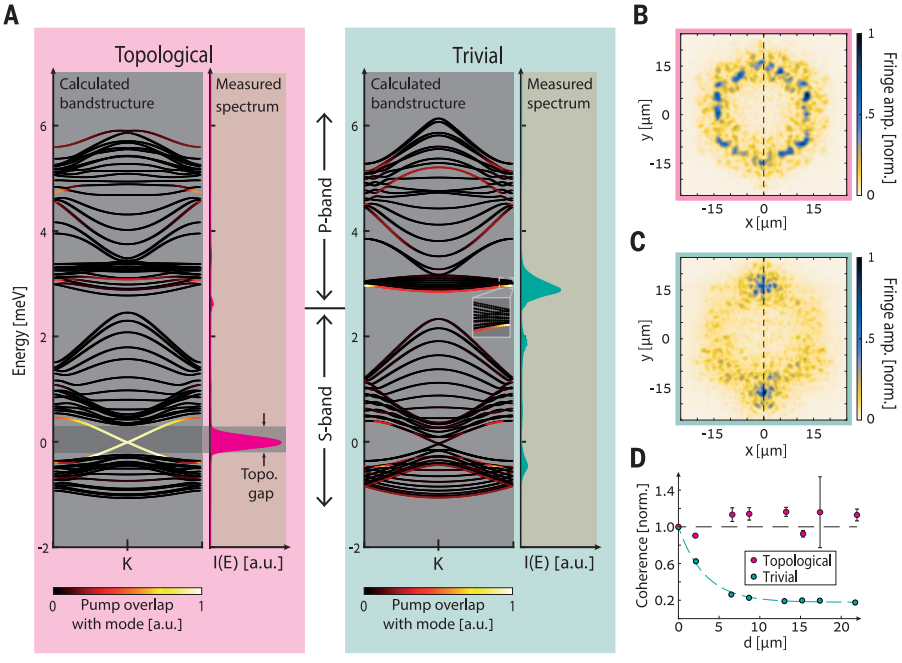

Fig. 4. Comparison between topological and trivial lasing in VCSEL arrays. (**A**) Calculated band structure of the photonic s- and p-bands of the topological and trivial arrays, along with the measured lasing spectra, I, as a function of energy E. The color of the bands indicates the overlap between the mode structure and the pump. Lasing in the topological array occurs exactly in the topological gap, where the group velocity is nonzero. This nonzero group velocity enables the injection locking of the VCSELs in the topological edge mode while suppressing lasing in localized groups of VCSELs. In the trivial array, lasing occurs in the lower edge of the p-band, where modes have group velocities approaching zero; hence, light does not circulate around the interface. Consequently, disorder causes lasing to occur in multiple independent groups of VCSELs, diminishing the mutual coherence. (**B** and **C**) Modulated part (fringe amplitude) of the mirror-interference measurements of the topological and trivial arrays, respectively. High modulation amplitude in each position is shown in (B), meaning that each of the 30 lasers of the topological interface is mutually coherent with its opposite partner. The graph in (C) displays coherence only near the mirror axis, which means that VCSELs that are far apart are not coherent with each other. The reason is lack of photonic transport in the trivial array, because the trivial edge modes have vanishing group velocity; hence, even weak disorder causes localized modes. (**D**) Modulation amplitude as a function of distance from the central VCSEL, averaged over all coherence paths and normalized to 1 at $d = 0$, extracted from (B) and (C). In the trivial case, coherence decays very rapidly, with a fit of ~3.5-μm decay length (dashed green). In the topological VCSEL array, high coherence is maintained around the whole interface. Error bars represent the standard deviation arising from local variations in fringe contrast.

and in doing that, it forces injection locking of all the VCSELs in that mode. It is therefore essential to examine the ability of VCSELs in the trivial array to interfere with one another, as we did for the topological array. Figure 4, B and C, shows the modulation amplitude extracted from the interference measurements, which is proportional to the mutual coherence of the array as a function of position. Comparing Fig. 4C with Fig. 4B, we notice a stark difference between the cases. The topological array shows coherence even for two lasers separated by half the interface length with three corners on its path, whereas the trivial honeycomb array results in coherence only around the autocorrelation points on the symmetry axis of the measurement, that is, only neighboring VCSELs show interference fringes. To compare the levels of coherence of the trivial and nontrivial arrays, we calculate the mean coherence as a function of the distance d from the VCSELs at $x = 0$ and normalize the coherence to 1 at $d = 0$ (where the central VCSEL interferes with itself) (Fig. 4D). The coherence of the topological insulator laser remains high along the whole path around the interface, whereas the trivial laser array shows the decay of coherence with increasing distance.

The topological VCSEL array separates between the vertical direction of lasing and the in-plane transport associated with the topological edge mode. This configuration endows the topological array with robustness for large variations of parameters. An immediate manifestation is shown in (*28*), where we examine the properties of the topological VCSEL array in a huge temperature range: between 4 and 200 K (fig. S7). The topological array also displays a narrow linewidth at 200 K, even though large temperature variations always change the refractive index and therefore the lasing wavelength. The linewidth of the topological VCSEL array remains narrow (~249 μeV) between 4 and 200 K (fig. S7C). This implies that the topological properties of this device are insensitive to changes in the wavelength. This happens because the topological VCSEL array scheme separates between the emission direction (where the DBRs and microcavity determine the wavelength) and the in-plane topological coupling, which are strongly coupled in all other schemes of topological insulator lasers.

The interference displayed in Fig. 3 confirms that our system is spatially coherent and that our topological 30-emitter VCSEL array acts as a single laser. The topologically protected transport, which is responsible for the injection locking of all the emitters, occurs in the plane of the chip—normal to the (vertical) direction of oscillation within each emitter. It is the topological design in which the VCSELs are positioned that forces all the emitters to act as a single laser. Research in topological photonics is now moving toward non-Hermitian and nonlinear topological phenomena, with the goal of using the properties of topological designs for new schemes of supreme semiconductor devices. The ability to separate between the direction of the topologically engineered platform and the oscillation direction within each emitter is a step toward this goal, offering the possibility to make large-scale coherent semiconductor laser arrays.

REFERENCES AND NOTES

1. G. Harari *et al*., in *Conference on Lasers and Electro-Optics (CLEO)* (OSA Technical Digest, Optical Society of America, 2016), paper FM3A.3.
2. G. Harari *et al*., *Science* **359**, eaar4003 (2018).
3. S. Wittek *et al*., in *Conference on Lasers and Electro-Optics (CLEO)* (OSA Technical Digest, Optical Society of America, 2017), paper FTh1D.3.
4. M. A. Bandres *et al*., *Science* **359**, eaar4005 (2018).
5. M. Hafezi, E. Demler, M. Lukin, J. Taylor, *Nat. Phys.* **7**, 907–912 (2011).
6. B. Bahari *et al*., *Science* **358**, 636–640 (2017).
7. Y. Zeng *et al*., *Nature* **578**, 246–250 (2020).
8. Z. K. Shao *et al*., *Nat. Nanotechnol.* **15**, 67–72 (2020).
9. Z.-Q. Yang, Z.-K. Shao, H.-Z. Chen, X.-R. Mao, R.-M. Ma, *Phys. Rev. Lett.* **125**, 13903 (2020).
10. Y. G. Liu, P. S. Jung, M. Parto, D. N. Christodoulides, M. Khajavikhan, *Nat. Phys.* **17**, 704–709 (2021).
11. J.-H. Choi *et al*., *Nat. Commun.* **12**, 3434 (2021).
12. I. Amelio, I. Carusotto, *Phys. Rev. X* **10**, 041060 (2020).
13. Z. Yang *et al*., *Phys. Rev. X* **10**, 011059 (2020).
14. D. E. Ackley, *Appl. Phys. Lett.* **42**, 152–154 (1983).
15. D. Botez, J. C. Connolly, *Appl. Phys. Lett.* **43**, 1096–1098 (1983).
16. S. S. Wang, H. G. Winful, *Appl. Phys. Lett.* **52**, 1774–1776 (1988).
17. H. G. Winful, S. S. Wang, *Appl. Phys. Lett.* **53**, 1894–1896 (1988).
18. R. K. DeFreez *et al*., *IEEE Photonics Technol. Lett.* **1**, 209–211 (1989).
19. H. G. Winful, *Phys. Rev. A* **46**, 6093–6094 (1992).
20. M. Orenstein *et al*., *Appl. Phys. Lett.* **58**, 804–806 (1991).
21. M. Orenstein, E. Kapon, J. P. Harbison, L. T. Florez, N. G. Stoffel, *Appl. Phys. Lett.* **60**, 1535–1537 (1992).
22. D. Francis, W. Yuen, H.-L. Chen, G. Li, C. Chang-Hasnain, *Electron. Lett.* **34**, 2132–2133 (1998).
23. F. Monti di Sopra *et al*., *Appl. Phys. Lett.* **77**, 2283–2285 (2000).
24. M. Miller, M. Grabherr, R. Jäger, K. J. Ebeling, *IEEE Photonics Technol. Lett.* **13**, 173–175 (2001).
25. H. Saito, K. Nishi, I. Ogura, S. Sugou, Y. Sugimoto, *Appl. Phys. Lett.* **69**, 3140–3142 (1996).
26. G. Edeltraud, O. Hess, *Spatio-Temporal Dynamics and Quantum Fluctuations in Semiconductor Lasers* (Springer, 2003).
27. P. Debernardi, G. P. Bava, C. Degen, I. Fischer, W. Elsasser, *IEEE J. Quantum Electron.* **38**, 73–84 (2002).
28. See supplementary materials.
29. L. Fu, *Phys. Rev. Lett.* **106**, 106802 (2011).
30. L. H. Wu, X. Hu, *Phys. Rev. Lett.* **114**, 223901 (2015).
31. G. Siroki, P. A. Huidobro, V. Giannini, *Phys. Rev. B* **96**, 041408 (2017).
32. Y. Yang *et al*., *Phys. Rev. Lett.* **120**, 217401 (2018).
33. X.-C. Sun, X. Hu, *Phys. Rev. B* **103**, 245305 (2021).

ACKNOWLEDGMENTS

M.S. would like to thank B. Shillman, the visionary founder of Congnex, for his continuing support for the Technion during crucial times. **Funding:** M.S. gratefully acknowledges an Advanced Grant from the European Research Council (ERC) under the European Union's Horizon 2020 research and innovation program (grant agreement no. 789339). The Würzburg group acknowledges financial support from the German Research Foundation (DFG) through the Würzburg-Dresden Cluster of Excellence on Complexity and Topology in Quantum Matter "ct.qmat" (EXC 2147, project ID 390858490). T.H.H. and S.H. acknowledge funding from the doctoral training program "Elitenetzwerk Bayern." T.H.H. acknowledges support from the German Academic Scholarship Foundation. The Würzburg team furthermore acknowledges support from the State of Bavaria. **Author contributions:** All authors contributed substantially to this work. **Competing interests:** Part of this work is included in a patent application filed by Technion and the University of Würzburg (international application no. PCT/IL2021/050489). **Data and materials availability:** All data needed to evaluate the conclusions in the paper are present in the paper and the supplementary materials.

SUPPLEMENTARY MATERIALS

https://science.org/doi/10.1126/science.abj2232
Materials and Methods
Figs. S1 to S7
References (*34*–*37*)

28 April 2021; accepted 17 August 2021
10.1126/science.abj2232

Topological insulator vertical-cavity laser array

Alex DikopoltsevTristan H. HarderEran LustigOleg A. EgorovJohannes BeierleinAdriana WolfYaakov LumerMonika EmmerlingChristian SchneiderSven HöflingMordechai SegevSebastian Klembt

Science, 373 (6562), • DOI: 10.1126/science.abj2232

Topologically locked for emission

The output power from a laser system can be increased by forming an array of lasers; however, because the individual lasers are independent, the resultant output may not be coherent. Dikopoltsev *et al*. report on the realization of a topological vertical-cavity surface-emitting laser (VCSEL) array. The topological nature of the array-based laser emission was achieved through a combination of topological in-plane propagation of evanescent light linking the vertical cavity surface-emitting lasers of the array. The topological features of the array force injection locking, making all emitters (30 in this case) act as a single coherent laser. This development will be important for realizing large-scale coherent laser arrays. —ISO

Science (ISSN) is published by the American Association for the Advancement of Science. 1200 New York Avenue NW, Washington, DC 20005. The title *Science* is a registered trademark of AAAS.